Journal of Membrane Science 561 (2018) 1–9

Contents lists available at ScienceDirect

Journal of Membrane Science

journal homepage: www.elsevier.com/locate/memsci

Temperature regulated reverse electrodialysis in charged nanopores

Rui Long*, Zhengfei Kuang, Zhichun Liu, Wei Liu*

School of Energy and Power Engineering, Huazhong University of Science and Technology, 1037 Luoyu Road, Wuhan 430074, China

ARTICLE INFO

Keywords:
Reverse electrodialysis
Temperature gradient
Nanopore

ABSTRACT

Nanofluidic reverse electrodialysis (RED) is a promising way to utilize the vastly existed salinity gradient energy. In this paper, impacts of temperature gradient across the nanopore on the ion transportation and power generation performance are systematically investigated, and a theoretical description has been derived to illustrate the energy conversion efficiency under asymmetric temperatures. Results reveal that under isothermal reservoirs, the maximum power increases with increasing temperatures, while the corresponding efficiency presents no obvious difference due to synchronous enhancement of the cation and anion diffusive coefficients. For salt solutions under asymmetric temperatures, at small concentration ratios, the larger average temperature, the larger maximum power output due to augmented enhanced ion transportation. A negative temperature gradient contributes to the maximum power efficiency while the positive one decreases the maximum power efficiency. At large concentration ratios, the nanofluidic RED system exhibits different behaviours. A negative temperature gradient contributes to the maximum power and the corresponding efficiency while the positive one decreases the maximum power and the corresponding efficiency. The results in this paper may offer desirable guidance for improving nanofluidic RED performance.

1. Introduction

Salinity gradient power generation, converting the Gibbs free energy of mixing into electricity, has drawn much attention due to vastly existed salinity gradient resources such as the mixing of sea and river water. Among them, reverse electrodialysis (RED) [1,2] and pressure retarded osmosis (PRO) [3] are promising methods for salinity gradient source utilization, and the former is more appealing due to relatively less demand on the system scale. In the RED system, ions diffuse from the high concentration reservoir to the low concentration one, split by an ion selective membrane, thus to induce a diffusive voltage for electricity extracted. In macro RED systems, choosing qualified ion selective membrane is of great important, however, the lack of high performance membrane, which induces rather small power density, hinders the commercial application. Recently, RED based on charged nanopores has shown its potential of attaining high power density [4,5]. Adjacent to the charged nanopore surface where co-ions are expelled and counter ions are attracted, the electric double layer (EDL) is formed, thus selective for the cations or anions based on the surface charge types. Kim et al. [6] obtained a power density 7.7 W/m^2 for the RED *via* a silica nanochannel, which is much larger than that obtained in macro RED systems, paving a new way for exploiting high performance nanofluidic RED systems. Kang et al. [7] achieve a power output density of 9.9 W/m^2 in anodic alumina nanopores. Feng et al. [8] demonstrated power density of up to 106 W/m^2 *via* the RED in a single-layer molybdenum disulfide nanopore. Guo et al. [9] achieved a maximum power output of 26 pW in an individual nanopore, and further claimed that power density can be enhanced by one to three orders over previous ion-exchange membranes, by adopting parallel nanopore arrays.

The performance of the nanofluidic RED mainly relies on the reservoir concentration, nanopore geometry and surface charateristics, salt types as well as pH [10–15]. Siria et al. [16] revealed a giant osmotic power density of 4 kW/m^2 in a single transmembrane boron nitride nanotube. Inspired by the electrical eel, wang et al.[17] proposed a high voltage nanofluidic RED system with voltage up to 1 V achieved by 20 alternatively multi-stacking cation and anion-exchange nanochannel network membranes. To elucidate of the role of steric effects, Esfandiar et al. [18] discussed the ion transport through ultimately narrow slits, and found that ions with hydrated diameters larger than the slit size can still permeate through. Tseng et al. [19] systematically investigated the influences of the nanopore size and the salt gradient on the nanofluidic RED performance, and revealed that a narrower and/or shorter nanopore, and a larger salt gradient lead to a larger power density, while a narrower and/or longer nanopore, and a smaller salt gradient are more appealing for a higher efficiency. Zhang et al. [20] demonstrated an engineered asymmetric bipolar structure membrane by combining a porous block copolymer membrane, polystyrene-*b*-poly

* Corresponding authors.
E-mail addresses: r_long@hust.edu.cn (R. Long), w_liu@hust.edu.cn (W. Liu).

https://doi.org/10.1016/j.memsci.2018.05.026
Received 24 March 2018; Received in revised form 4 May 2018; Accepted 14 May 2018
Available online 16 May 2018
0376-7388/ © 2018 Elsevier B.V. All rights reserved.

with a track-etched asymmetric porous polyethylene terephthalate membrane to eliminate the concentration polarization phenomenon, and the power density was considerably increased. Cao et al. [21] investigated the impacts of nanopore length on the nanofluidic RED system, and found that at short nanopore length, the system demonstrates an anomalous, non-Ohmic response due to the fact that excessively short channel length impairs the charge selectivity and induces strong ion concentration polarization. They further claimed that the optimal channel length should be between 400 and 1000 nm to balance the power extracted and energy efficiency. Zhang et al. [22] further revealed that using slippery nanopores, the energy efficiency at the short nanopore length could be dramatically increased under large salt concentrations.

Aforementioned efforts focusing on the nanofluidic RED system mainly deal with the isothermal salt solution reservoirs [23]. The asymmetric temperature of the solution reservoirs has been rarely considered for the nanofluidic RED systems, which has shown its potential in tuning ion transportation in nanochannels. Provided temperature gradient applied, due to the Soret effects, ions diffuse along or opposite to the temperature gradient stemming from their different thermal responsiveness [24,25]. Ghonge et al. [26] investigated the flow through a narrowparallel-plate channel with the temperature gradients. Wood et al. [27] studied the influence of the Joule heating, viscous dissipation and imposed temperature gradients on a nanochannel system, and found that the effects of Joule heating and viscous dissipation only become relevant for higher salt concentrations and electric field strengths. Benneker et al. [28] investigated the influence of applied temperature difference electric fields over tapered nanochannels on the flow behaviour, and found that applying a temperature gradient along the electric field enhances the selectivity of the tapered channels while a temperature gradient countering the electric field reduces the selectivity.

In this paper, we focused on the temperature gradient across the negatively charged nanopore on the performance of nanofluidic RED systems described by the Poisson–Nernst–Planck equations and Navier-Stocks equations as well as energy conservation equation to illustrate the electrostatics, ionic mass transport, heat transfer and hydrodynamics process. The impact of concentration gradient direction, temperature gradient direction, nanopore size on the transference number, membrane potential, osmotic current, maximum power, and maximum power density are investigated, and the underlying mechanisms are discussed in detail. The obtained results could provide useful information to improving the performance of nanofluidic RED systems.

2. Theory

As depicted in Fig. 1(a), we consider a cylindrical nanopore with radius R_n and length L_n in a solid membrane, which contacts with two same large reservoirs (NaCl aqueous solution) of radius $R_r = 500$ nm and length $L_r = 500$ nm at salt concentrations C_H and C_L ($C_H > C_L$), and temperatures T_H and T_L, respectively. The membrane wall of the nanopore is charged with constant charge density σ, and the others are free of charge. The continuum based model coupling Poisson-Nerst-Planck equations, Navier-Stockes equations and energy conservation equation is employed to illustrate the electrostatics, ionic mass transport, heat transfer and energy transportation characteristics. Relevant governing equations are summarized below [29,30].

$$-\varepsilon\nabla^2\phi = F\sum_{i=1}^{2} z_i c_i \tag{1}$$

$$\nabla\cdot\boldsymbol{J}_i = 0\ ,\ \text{where}\ \boldsymbol{J}_i = c_i\boldsymbol{u} - D_i\nabla c_i - \frac{D_i z_i F c_i}{RT}\nabla\phi - \frac{2D_i\alpha_i c_i}{T}\nabla T \tag{2}$$

$$-\nabla p + \mu\nabla^2\boldsymbol{u} - F\sum_{i=1}^{2} z_i c_i\nabla\phi - \frac{1}{2}|\boldsymbol{E}|^2\nabla\varepsilon = 0 \tag{3}$$

$$\nabla\cdot\boldsymbol{u} = 0 \tag{4}$$

$$\rho C_p\boldsymbol{u}\cdot\nabla T = k\nabla^2 T \tag{5}$$

where ϕ is the electrical potential. $\boldsymbol{J}_i$, c_i, D_i and z_i are the ionic flux, concentration, diffusivity, and valence of the ith ionic species, respectively ($i = 1$ for Na^+ and $i = 2$ for Cl^-). α_i is the reduced Soret coefficient, which is defined as $\alpha = TS_T/2$, where S_T represents the intrinsic Soret coefficients of cations or anions in the absence of charge coupling [31]. $\alpha = 0.7$ for Na^+ and $\alpha = 0.1$ for Cl^- [24]. F, R and T are the Faraday constant, universal gas constant and the fluid temperature. ε, p, and $\boldsymbol{u}$ are the permittivity, pressure, and velocity of the fluid. ρ, C_p,and k are the density, specific capacity, and thermal conductivity. $E = -\nabla\phi$ is the electric field. As presented in Eq. (2), the ionic flux consists of the convective, ionic diffusive, electrodiffusive and thermodifussive fluxes, respectively corresponding to the first, second, third and last terms in the right hand. In Eq. (3), the electrostatic force and the electrothermal force (dielectric force) are also considered to include the impact of the temperature gradient across the nanopore. The temperature depended properties of the salt solutions are listed in the Appendix A.

To solve the above equations, proper boundary conditions are needed. Actually surface charge density is impacted by the temperature [32]. The relation of temperature and the surface charge density is kind of complex. In present study the assumption of constant surface charge density $\sigma = -10mC/m^2$ at the negatively charged membrane wall is employed, which has been adopted in many previous literatures [28,33]. And the reservoir wall is free of charge $\sigma = 0$. The wall of the nanopore and that of the reservoir are impermeable to ions. Ω_n are non-slip and Ω_r is slip, where Ω_n,and Ω_r are the surface of the nanopore and the reservoir. Therefore, the following boundary conditions apply.

$$-\varepsilon\boldsymbol{n}\cdot\nabla\phi = 0 \text{ on } \Omega_r \text{ and } \Lambda_j \tag{6}$$

$$-\varepsilon\boldsymbol{n}\cdot\nabla\phi = \sigma \text{ on } \Omega_n \tag{7}$$

$$\boldsymbol{n}\cdot\boldsymbol{J}_i = 0 \text{ on } \Omega_r \text{ and } \Lambda_j \tag{8}$$

$$T = T_j \text{ at } \Lambda_j \tag{9}$$

where $\boldsymbol{n}$ is the normal vector Λ_j represents the reservoir end.

The electric current is calculated by

$$I = \int_{\Lambda} F\Big(\sum_{i=1}^{2} z_i\boldsymbol{J}_i\Big)\cdot\boldsymbol{n}d\Lambda \tag{10}$$

The transference number (t_+) indicating the nanopore selectivity can be calculated as

$$t_+ = \frac{I_1}{I_1 + |I_2|} \tag{11}$$

where I_1 and I_2 are the electrical current stepping from the cation and anion, respectively.

The simulations are performed using the commercial Multiphysics software COMSOL. The behaviour of the system is examined by numerical simulation through varying the nanopore radius, length, and reservoir temperature and concentration based on the finite element method with quadrilateral elements and refined meshes with 310,000 elements. The calculation results are confirmed to the grid independent solution by solutions obtained from denser meshes (see the Appendix A).

3. Results and discussion

As shown in Fig. 1(b), under the presence of temperature gradient, the voltage still presents a linear relationship with the electric current, indicating the system exhibits the Ohm behaviour. Therefore, the

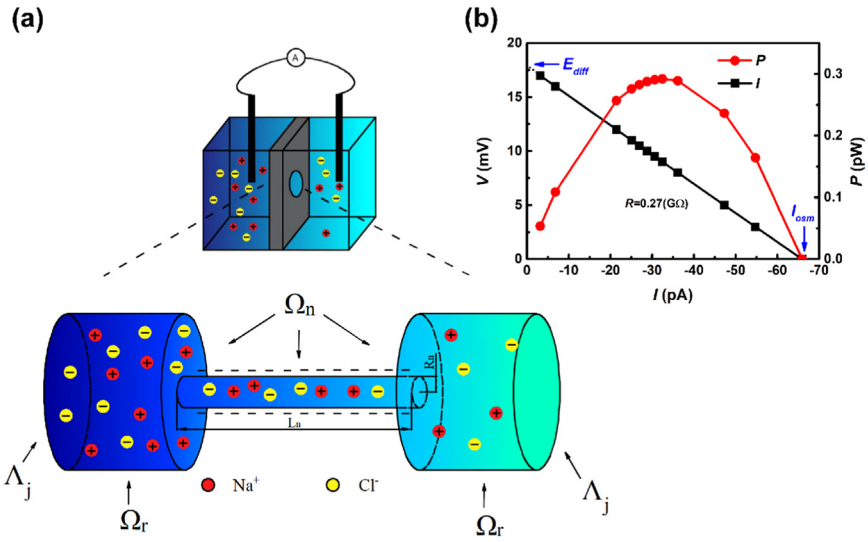

Fig. 1. (a) Schematic of the nanofluidic RED system through a cylindrical nanopore with length L_n, and radius R_n. The nanopore connects two same, large cylindrical reservoirs at salt concentrations C_H and C_L ($C_H > C_L$), and temperatures T_H and T_L, respectively. The calculation domain is presented below and no electrode reactions are considered. There exist two configurations for the ion transportation: (I) High concentration and temperature are employed at the same reservoir, (II) High concentration and low temperature are employed at the same reservoir. In addition, the simulated current-voltage curve and current-power curve are also plotted (b) at $\sigma = -10\text{mC}/m^2$, $T_H = 320$ K, $T_L = 300$ K, $C_H = 50$ mM, $C_L = 1$ mM, $R_n = 10$ nm, and $L_n = 800$ nm.

membrane potential (the voltage under which the net diffusion current is zero) can be obtained by linear extrapolation. The harvestable electric power is the product of the ionic current (I) and the output potential (V), which achieves its maximum value obtained by Ohm's law when the output voltage is the half of the membrane potential [34]

$$P_{\max} = \frac{I_{osm} E_{diff}}{4} \tag{12}$$

Fig. 2 shows the osmotic current under different temperature gradients and nanopore sizes. For isothermal reservoirs, the lager temperature, the larger osmotic current due to synchronously enhanced diffusive coefficients, which contribute to the ion transportation as shown in Fig. 3. To include the impacts of the asymmetric temperature across the nanopore on the ions transportation, we consider the Soret effect induced by the temperature gradient, which drives the ions to aggregate into the hot or cold sides according to the positive or negative sign of the reduced Soret number. A positive sign means that ions (such as Na^+ and Cl^- in present study) prefer to move towards the cold side. As the ions diffuse from the high concentration reservoir to the low concentration one, a positive temperature gradient (the same direction as the concentration gradient) induces the ion aggregation of the Na^+ and Cl^- in the nanopore due to decreased diffusive coefficient along the ion transportation direction, as shown in Fig. 4 and Fig. 5. Moreover, a negative temperature gradient leads to less ion concentrations in the nanopore. This is ascribed to that a positive temperature gradient indicates the cold side is the low concentration reservoir, where the diffusive coefficient is much lower than the hot side (high concentration side), ions will aggregate in the nanopore and the osmotic flux is

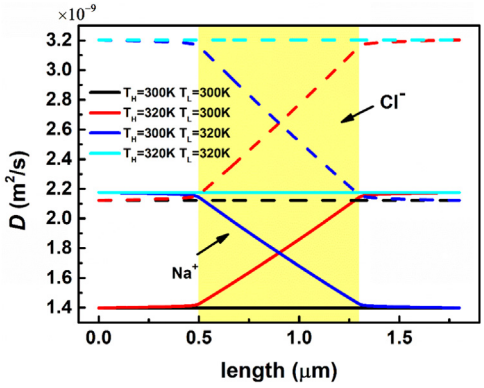

Fig. 3. Ion diffusive coefficients for Na^+ and Cl^- in the axial direction, where $R_n = 10$ nm, $L_n = 800$ nm, and $\sigma = -10\text{mC}/m^2$.

decreased as depicted in Fig. 6. When a negative temperature gradient applied, along the ion transportation direction, the diffusive coefficients increases gradually, which contributes to ion diffusion across the nanopore. Therefore, the osmotic flux at the negative temperature gradient is larger than that at the positive one, thus a larger osmotic current. Furthermore, due to reduced EDL overlapping degree at larger nanopore radius, the osmotic current decreases. We can also see that under the same a shorter nanopore length leads to a larger osmotic current due to enhanced concentration gradient.

At low concentration ratios such as $C_H/C_L = 10$, the ion diffusion is

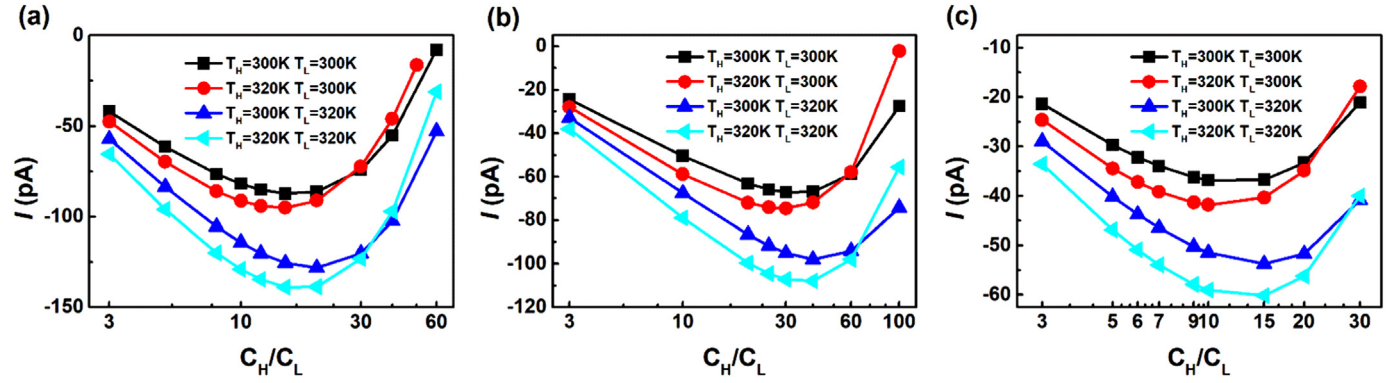

Fig. 2. Variation of osmotic current with the concentration ratios (C_H/C_L) for different combinations of R_n and L_n at different temperature gradients with a surface charge density of $\sigma = -10\text{mC}/m^2$. (a) $R_n = 10$ nm, $L_n = 300$ nm; (b) $R_n = 10$ nm, $L_n = 800$ nm; (c) $R_n = 20$ nm, $L_n = 800$ nm.

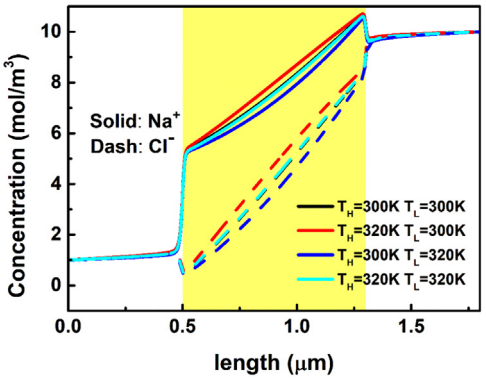

Fig. 4. Axial concentration distribution for Na^+ (c_1) and Cl^- (c_2) along ion transportation direction where $C_H/C_L = 10$, where $R_n = 10$ nm, $L_n = 800$ nm, and $\sigma = -10\text{mC}/m^2$.

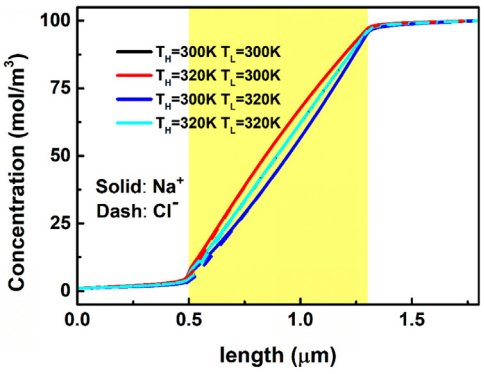

Fig. 5. Axial concentration distribution for Na^+ (solid) and Cl^- (dash) along ion transportation direction where $C_H/C_L = 100$, where $R_n = 10$ nm, $L_n = 800$ nm, and $\sigma = -10\text{mC}/m^2$.

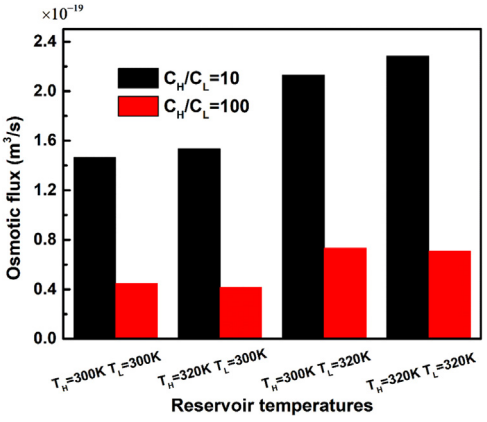

Fig. 6. Osmotic volume flux under asymmetric reservoir temperatures, where $R_n = 10$ nm, $L_n = 800$ nm, and $\sigma = -10\text{mC}/m^2$.

rather weak. The EDL overlapping is dominant and the Cl^- transportation is hindered by the electrostatic force. A positive temperature gradient still results in a small increase of the osmotic current due to enhance diffusive coefficient at elevated temperatures, as depicted in Fig. 3 and Fig. 6. However, at high concentration ratios such as $C_H/C_L = 100$, the EDL is much thinner, and the diffusive effect is enhanced. As the diffusive coefficient of Cl^- is larger than that of the Na^+, while the reduced Soret coefficient of Na^+ is much larger than Cl^- indicating Na^+ mitigates to the cold side more quickly, at the positive temperature gradient, the concentration difference of the Na^+ and Cl^- is decreased. Therefore, the less net charge density leads to a reduced osmotic flux and current, as shown in Fig. 2 and Fig. 6. The osmotic current under $T_H = 320$ K and $T_L = 300$ K is less than that under $T_H = T_L = 300$ K. When a negative temperature gradient applied, the ion transportation driven by the concentration gradient is opposite to that driven by the thermophoretic force induced by the temperature gradient. The concentration difference is augmented, thus to result in a larger osmotic current, as depicted in Fig. 2 where the osmotic current under $T_H = 300$ $T_L = 320$ is larger than that under $T_H = T_L = 320$ K. Although a shorter length leads to a larger osmotic current, it decreases the transference number due to increased concentration polarization.

Fig. 7 shows the transference number decreases monotonously with increasing concentration ratios. At isothermal reservoirs with absence of thermodiffusive effects, the transference number is not obviously impacted by the temperature due to the fact that the diffusive coefficients of the Na^+ and Cl^- are enhanced simultaneously at elevated temperatures as shown in Fig. 3, where the axial concentration distribution for Na^+ (Cl^-) at different temperatures coincides with each other. When a positive temperature gradient applied, both Na^+ and Cl^- concentrations increase, but the later (Cl^-) is increased much more significantly, indicating weakened ion selectivity. When a negative temperature gradient is applied, although the Na^+ and Cl^- concentrations both decreases while the decrease of the Cl- is much more obvious, resulting in enhanced selectivity, as shown in Fig. 4 and Fig. 5.

Fig. 8 presents the membrane potential first increases with increasing concentration ratio, reaches its maximum value, then decreases, which has been reported in previous literatures [15,35]. The membrane potential can be written approximatively as

$$E_{diff} = (2t^+ - 1)\frac{R\overline{T}}{zF}\ln\left(\frac{\gamma_H C_H}{\gamma_L C_L}\right) \tag{13}$$

Although under isothermal reservoirs, the transference number does not show much difference, the membrane potential at 320 K is larger than that at 300 K due to elevated solution temperature based on Eq. (13). For reservoirs with asymmetric temperatures, the impact of transference number is more significant than the average solution temperature, thus the relative magnitude of the membrane potential at different configurations present the same trend as the transference number. Larger transference number leads to larger membrane potential. The positive temperature gradient induces more Cl^- in the nanopore, thus a much less transference number and membrane potential. A negative temperature gradient results in much less Cl^- in the nanopore, thus a larger transference number and membrane potential. In addition, for the nanopore of $R_n = 10$ nm and $L_n = 800$ nm, the optimal concentration ratio for maximum osmotic current is around 30, while the optimal concentration ratio for maximum membrane potential is around 10, which stems from that large concentration ratio contributes to the ions transportation while it is adverse to the membrane potential induced by decreased ion selectivity.

Fig. 9 shows that the maximum power first increases with increasing concentration ratio, reaches its maximum value, then decreases. Due to the existence of optimal concentration ratios respectively, leading to the maximum osmotic current and membrane potential, there should also exist an optimal concentration ratio leading to the maximum value of the maximum power extracted. As at low concentration ratios, the osmotic current is more sensitively to the involved temperature, larger average temperature leads to larger value of the maximum power output. At high concentration ratios, a negative gradient temperature contributes to the maximum power output while the positive temperature difference acts against the maximum power extracted due to decreased osmotic current and membrane potential attributed to the coupling impacts of the thermodiffusion and the concentration gradient driven diffusion.

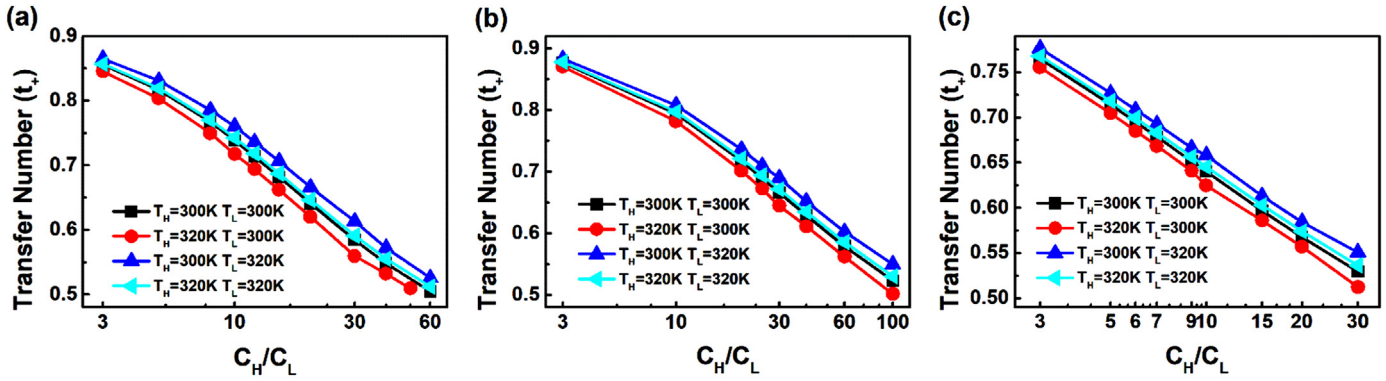

Fig. 7. Variation of transference number (t_+) with the concentration ratios (C_H/C_L) for different combinations of R_n and L_n at different temperature gradients with a surface charge density of $\sigma = -10\text{mC}/m^2$. (a) $R_n = 10$ nm, $L_n = 300$ nm; (b) $R_n = 10$ nm, $L_n = 800$ nm; (c) $R_n = 20$ nm, $L_n = 800$ nm.

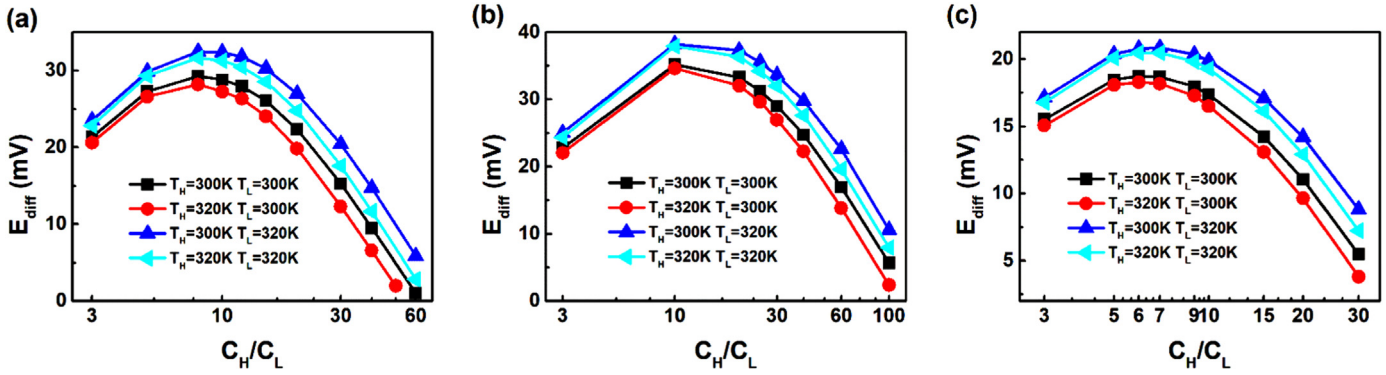

Fig. 8. variation of membrane potential with the concentration ratios (C_H/C_L) for different combinations of R_n and L_n at different temperature gradients with a surface charge density of $\sigma = -10\text{mC}/m^2$. (a) $R_n = 10$ nm, $L_n = 300$ nm; (b) $R_n = 10$ nm, $L_n = 800$ nm; (c) $R_n = 20$ nm, $L_n = 800$ nm.

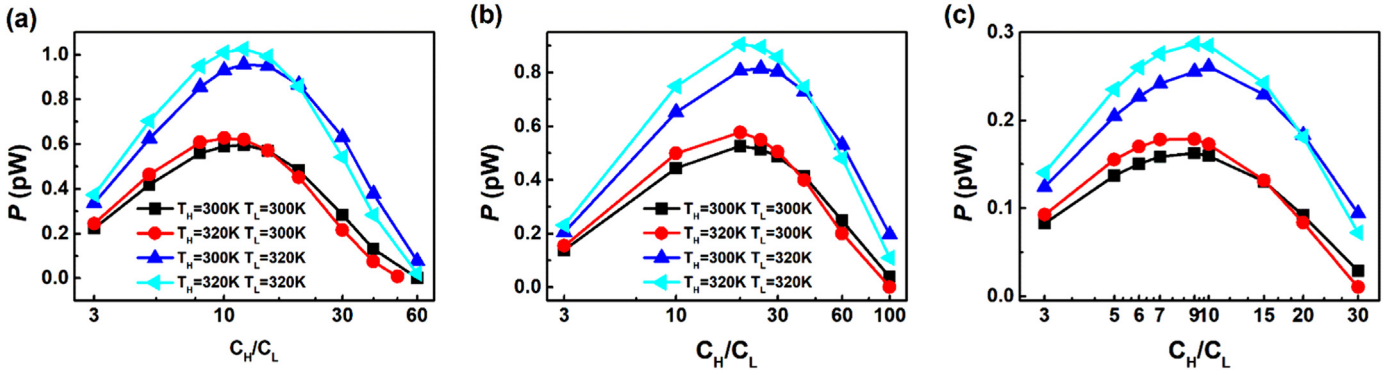

Fig. 9. Variation of maximum power with the concentration ratios (C_H/C_L) for different combinations of R_n and L_n at different temperature gradients with a surface charge density of $\sigma = -10\text{mC}/m^2$. (a) $R_n = 10$ nm, $L_n = 300$ nm; (b) $R_n = 10$ nm, $L_n = 800$ nm; (c) $R_n = 20$ nm, $L_n = 800$ nm.

3.1. Maximum power efficiency under asymmetric temperature gradients

The energy conversion efficiency at maximum power condition can be derived based on the themordynamic diffusion theory. Considering the ion diffusion from the high concentration solution at concentration C_H and temperature T_H to the low concentration solution at concentration C_L and temperature T_L. At the steady state, the flux of Gibbs free energy consumed is [9]

$$\Delta\dot{G} = \Delta\dot{G}_H + \Delta\dot{G}_L = (\mu_{+,H} - \mu_{+,L})\dot{n}_{+,H} + (\mu_{-,H} - \mu_{-,L})\dot{n}_{-,H} \tag{14}$$

where + and - denotes the cation (Na^+) and anion (Cl^-) respectively. μ and $\dot{n}$ are chemical potential and ion flux, given by [36]

$$\mu_{i,j} = \mu_{i,0} + RT_j \ln \beta_j \tag{15}$$

$$\dot{n}_{i,H} = -\frac{|I_i|}{F} \tag{16}$$

where I_i is the current contributed by the cation (i is +) or anion (i is –). j denotes high concentration (H) or low concentration (L).

Therefore the flux of Gibbs free energy consumption is

$$\Delta G = \sum_i (RT_H \ln \beta_{i,H} - RT_L \ln \beta_{i,L})\frac{I_i}{F} \tag{17}$$

The power achieves its maximum value $P_{\max} = (|I_+| - |I_-|)V$, at $V = E_{diff}/2$. The energy efficiency at maximum power is defined as the ratio of the retrievable electric power to the Gibbs free energy of mixing

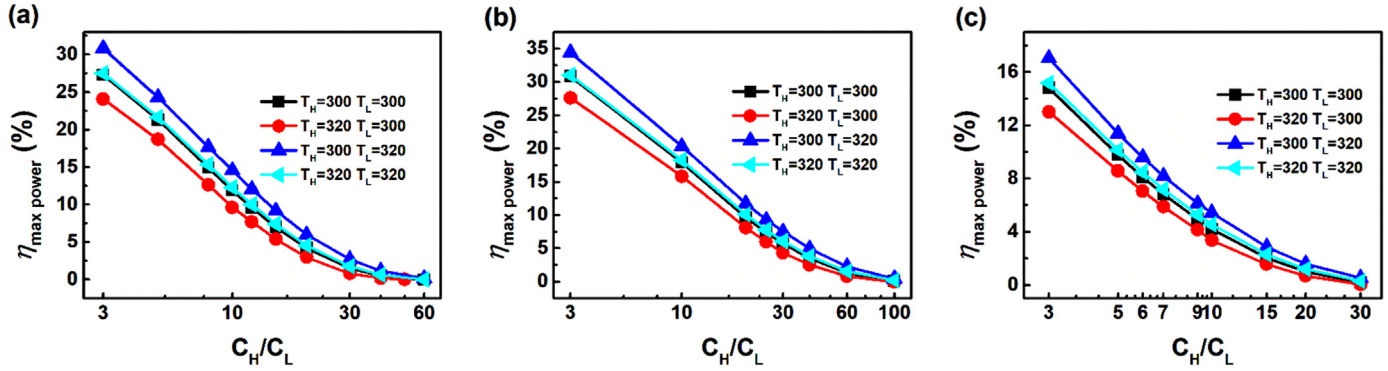

Fig. 10. variation of maximum power efficiency with the concentration ratios (C_H/C_L) for different combinations of R_n and L_n at different temperature gradients with the surface charge density of $\sigma = -10\mathrm{mC}/m^2$. (a) R_n = 10 nm, L_n = 300 nm; (b) R_n = 10 nm, L_n = 800 nm; (c) R_n = 20 nm, L_n = 800 nm.

$$\eta = \frac{(|I_+| - |I_-|)\frac{E_{diff}}{2}}{\frac{R}{F}\ln\frac{\beta_{+,H}{}^{T_H}}{\beta_{+,L}{}^{T_L}}|I_+| + \frac{R}{F}\ln\frac{\beta_{-,H}{}^{T_H}}{\beta_{-,L}{}^{T_L}}|I_-|} \tag{18}$$

Applying $\frac{\beta_{+,H}{}^{T_H}}{\beta_{+,L}{}^{T_L}} = \frac{\beta_{-,H}{}^{T_H}}{\beta_{-,L}{}^{T_L}} = \frac{\beta_H{}^{T_H}}{\beta_L{}^{T_L}}$ and $|I_+|/|I_-| \cong t_+/(1-t_+)$, the maximum power efficiency is

$$\eta = \frac{(2t_+ - 1)\frac{E_{diff}}{2}}{\frac{R}{F}\ln\frac{(C_H\gamma_H)^{T_H}}{(C_L\gamma_L)^{T_L}}} \tag{19}$$

where γ_H and γ_L are the activity coefficient of the high and low concentration solutions, which could be calculated by [37]

$$\log(\gamma_{H(L)}{}^{1/z_+z_-}) = \frac{-0.511I_s{}^{1/2}}{1 + I_s{}^{1/2}} + \frac{(0.06 + 0.03444)I_s}{(1 + \frac{1.5}{|z_+z_-|}I_s)^2} + \frac{0.0574I_s}{|z_+z_-|} \tag{20}$$

where I_s is the ionic strength.

Fig. 10 shows the maximum power efficiency decreases with increasing concentration ration due to decreased transference number based on Eq. (19). As the negative temperature gradient contributes to the transference number and decreases the Gibbs free energy consumed, thus a larger value of maximum power efficiency is achieved. On the contrary, a positive temperature gradient goes against the transference number and enhances the Gibbs free energy consumption, hence leads to a reduced maximum power efficiency, as shown in Fig. 10.

4. Conclusions

In this paper, the impacts of temperature gradient across the nanopore on the ion transportation and performance of nanofluidic RED are systematically investigated. Results reveal that under isothermal reservoirs, the maximum power increases with increasing reservoir temperature, but the maximum power efficiency presents no obvious difference under elevated temperatures. For the nanofluidic RED with reservoirs at asymmetric temperatures, at small concentration ratios, the larger average temperature, the larger maximum power output, due to enhanced ion transportation. However, a negative temperature gradient contributes to the maximum power efficiency and the positive one decreases the maximum power efficiency. For the nanopore of R_n = 10 nm and L_n = 800 nm, at a concentration ratio of C_H/C_L = 3, the maximum power is increased by 11.1% and 48.4%, respectively, under the positive and negative temperature gradients comparted to that under T_H = T_L = 300 K. The maximum power efficiency is increased by 11.6% under the negative temperature gradient (T_L = 320 K and T_H = 300 K) and is decreased by 10.5% under the positive temperature gradient (T_H = 320 K and T_L = 300 K). At larger concentration ratios, the nanofluidic RED system exhibits different behaviours. A negative temperature gradient contributes to the maximum power and the corresponding efficiency and the positive one decreases the maximum power and the corresponding efficiency. For the nanopore of R_n = 10 nm and L_n = 800 nm, at a concentration ratio of C_H/C_L = 100, the maximum power and the maximum power efficiency are increased by 79.2% and 135% under the negative temperature gradient (T_L = 320 K and T_H = 300 K) comparted to those under T_H = T_L = 320 K. The maximum power and the maximum power efficiency are decreased by 96.7% and 97.5% under the positive temperature gradient (T_H = 320 K and T_L = 300 K).

Acknowledgements

We acknowledge the support received from the National Natural Science Foundation of China (51706076, 51736004).

Appendix A

A1 Temperature depended properties

The temperature depended relative permittivity (ε_r) is [38,39]

$$\varepsilon_r = \exp(4.47615 - 4.60128 \times 10^{-3}\Delta T + 2.6952 \times 10^{-7}(\Delta T)^2) \tag{A1}$$

where $\Delta T = T - 273.15$, $0 \le \Delta T \le 100$.

The temperature depended viscosity is [23]

$$\mu = 2.414 \times 10^{-5} \times 10^{247.8/(T-140)},\ 273.15 \le T \le 643.15 \tag{A2}$$

Based on the Nernst-Haskell equation, the diffusive coefficient D_i (i = 1 for Na^+ and i = 2 for Cl^-) is [23,40]

$$D_i = \frac{RT}{F^2}\left[\frac{1/|z_i|}{1/\lambda_i^0}\right] \tag{A3}$$

where the λ_i^0 is the ionic limiting conductance given by [23]

$$\lambda_i^0 = \lambda_i^0 + a\Delta T + b(\Delta T)^2 + c(\Delta T)^3 \tag{A4}$$

where λ_i^0 is the limiting conductance at temperature $T = 298.15K$. $-20 \leq \Delta T = T - 298.15 \leq 30$. The values for a, b and c for Na^+ and Cl^- are listed in Table A1

Table A1
Values of the parameters used in Eq. (4) [23].

	$\lambda_i^0(298.15K)$	a	b	c
Na^+	50.15	1.09160	0.4715×10^{-2}	-0.115×10^{-4}
Cl^-	76.35	1.54037	0.465×10^{-2}	-0.1285×10^{-4}

A2 Model validity

See Fig. A1

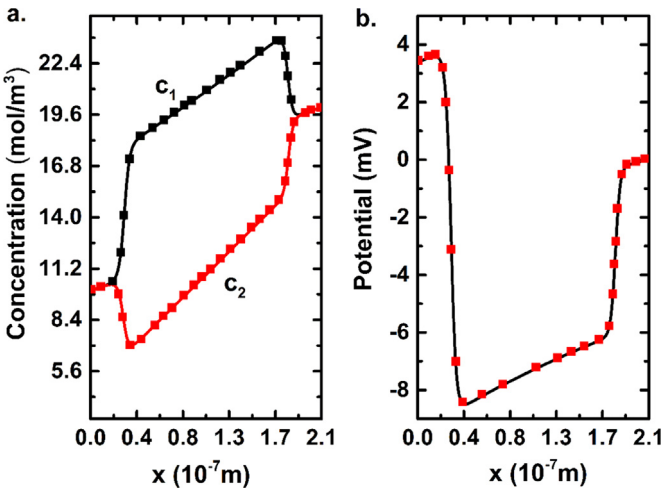

Fig. A1. Concentration of the cation (c_1) and anion (c_2) ions (a) and the induced electric potential along the x-axis of the nanochannel. The lines and square symbols represent, respectively, our numerical results and those obtained by Pivoka and Smith [41]. In the calculation, the nanochannel radius is 5 nm with length 150 nm, the salt concentrations in the reservoirs are, respectively, 10 mM and 20 mM. The charge density of the nanopore wall is -0.01C/m^2. The diffusivity of the cation ion is 3.0×10^{-9} m^2/s and that of the anion ion is 1.5×10^{-9} m^2/s. The validation of our calculation can be justified by great agreement between our numerical results and those obtained by Pivoka and Smith [41].

A3 Grid independence

We calculated the osmotic current under different grid numbers, where $C_H = 30$ mM, $C_L = 1$ mM and $T_H = T_L = 300$ K. The pore radius is 10 nm and the length is 800 nm. We found that when the gird number is *ca.* 310000, the value of osmotic current is stable, which is the same as that obtained under the grid number of *ca.* 410000. Therefore, for all the calculation in present study, a grid number of *ca.* 310000 was employed.

See Table A2

Table A2
Osmotic current under different grid numbers.

Grid number	160000	230000	310000	410000
Osmotic current (nA)	0.0670	0.0671	0.0672	0.0672

A4 Ionic current rectification

See Fig. A2

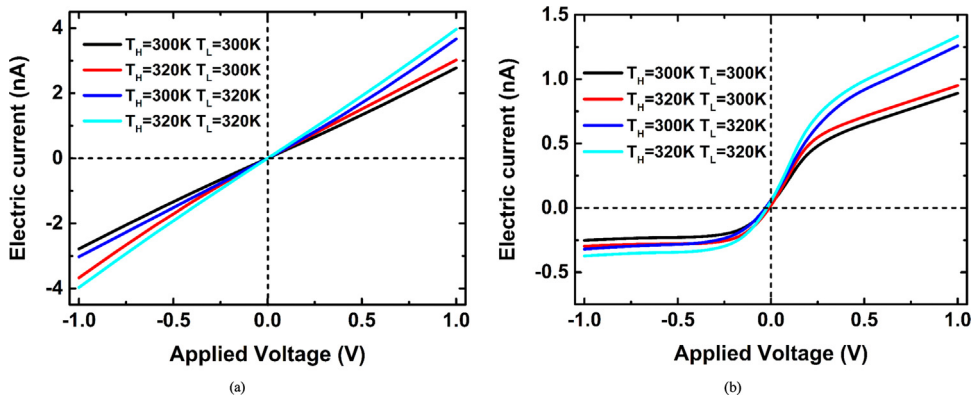

Fig. A2. Rectified ion transport through the negatively charged nanopore under different temperature gradients, where R_n = 10 nm, L_n = 800 nm, σ = 10mC/m^2, C_H=C_L= 10 mM (a) C_H= 60 mM, C_L= 1 mM (b). As shown in Fig. A1 (a) where no concentration gradient is applied, under isothermal conditions, no ionic rectification can be observed, while under asymmetric temperatures, the charged nanopore presents a certain slight ionic rectification. In previous studies, under isothermal conditions, ionic rectification can not be observed in the cylinder with symmetric geometry due to unchanged viscosity and ion diffusive coefficients. In present study with asymmetric temperatures, the viscosity and the ion diffusive coefficients are uneven in the nanopore, which are responsible for the ICR phenomenon. When concentration gradient imposed across the nanopore, ICR phenomenon is observed under isothermal and non-isothermal conditions as shown in Fig. A1 (b). We can see that the direction of the temperature gradient has significant impact on the ion selectivity. A reversed temperature gradient contributes to the ICR, which is mainly determined by the temperature depended property of the ion diffusive coefficients.

A5 cation/anion electrical current contributions

The cation/anion electrical current contributions of different fluxes are shown in Table A3, where C_H= 30 mM, C_L= 1 mM. The pore radius is 10 nm and the length is 800 nm. We can see that the convective current, diffusive current, electrodiffusive current and the thermodifussive current are all temperature-depended. The current contribution of the thermodifussive effect is very small and negligible compared to the diffusive current and the electrodiffusive current.

Table A3
Cation/anion electrical current contributions.

Reservoir temperatures	Cation/anion current	Convective current (pA)	Diffusive current (pA)	Electrodiffusive current (pA)	Thermodifussive current (pA)
T_H= 300 K	$I_{1,j}$	12.05	79.77	42.91	0.00
T_L= 300 K	$-I_{2,j}$	12.05	120.65	− 65.14	0.00
T_H= 320 K	$I_{1,i}$	12.42	97.89	47.65	4.66
T_L= 300 K	$-I_{2,j}$	12.42	145.96	− 71.33	0.98
T_H= 300 K	$I_{1,j}$	17.77	101.07	58.98	− 3.42
T_L= 320 K	$-I_{2,j}$	17.77	150.43	− 88.17	− 0.74
T_H= 320 K	$I_{1,j}$	18.78	124.27	66.83	0.00
T_L= 320 K	$-I_{2,j}$	18.78	182.31	− 98.39	0.00

References

[1] R. Long, B. Li, Z. Liu, W. Liu, Hybrid membrane distillation-reverse electrodialysis electricity generation system to harvest low-grade thermal energy, J. Membr. Sci. 525 (2017) 107–115.

[2] R. Long, B. Li, Z. Liu, W. Liu, Reverse electrodialysis: modelling and performance analysis based on multi-objective optimization, Energy 151 (2018) 1–10.

[3] R. Long, X. Lai, Z. Liu, W. Liu, A continuous concentration gradient flow electrical energy storage system based on reverse osmosis and pressure retarded osmosis, Energy 152 (2018) 896–905.

[4] A. Esfandiar, B. Radha, F. Wang, Q. Yang, S. Hu, S. Garaj, R. Nair, A. Geim, K. Gopinadhan, Size effect in ion transport through angstrom-scale slits, Science 358 (2017) 511–513.

[5] J. Hwang, S. Kataoka, A. Endo, H. Daiguji, Enhanced energy harvesting by concentration gradient-driven ion transport in SBA-15 mesoporous silica thin films, Lab Chip 16 (2016) 3824–3832.

[6] D.-K. Kim, C. Duan, Y.-F. Chen, A. Majumdar, Power generation from concentration gradient by reverse electrodialysis in ion-selective nanochannels, Microfluid. Nanofluidics 9 (2010) 1215–1224.

[7] B.D. Kang, H.J. Kim, M.G. Lee, D.-K. Kim, Numerical study on energy harvesting from concentration gradient by reverse electrodialysis in anodic alumina nanopores, Energy 86 (2015) 525–538.

[8] J. Feng, M. Graf, K. Liu, D. Ovchinnikov, D. Dumcenco, M. Heiranian, V. Nandigana, N.R. Aluru, A. Kis, A. Radenovic, Single-layer MoS_2 nanopores as nanopower generators, Nature 536 (2016) 197.

[9] W. Guo, L. Cao, J. Xia, F.-Q. Nie, W. Ma, J. Xue, Y. Song, D. Zhu, Y. Wang, L. Jiang, Energy harvesting with single-ion-selective nanopores: a concentration-gradient-driven nanofluidic power source, Adv. Funct. Mater. 20 (2010) 1339–1344.

[10] H. Zhang, Y. Tian, L. Jiang, Fundamental studies and practical applications of bioinspired smart solid-state nanopores and nanochannels, Nano Today 11 (2016) 61–81.

[11] J.P. Hsu, S.T. Yang, C.Y. Lin, S. Tseng, Ionic current rectification in a conical nanopore: influences of electro osmotic flow and type of salt, J. Phys. Chem. C 121 (2017) 4576–4582.

[12] J.P. Hsu, H.H. Wu, C.Y. Lin, S. Tseng, Ion current rectification behavior of bioinspired nanopores having a pH-tunable zwitterionic surface, Anal. Chem. 89 (2017) 3952–3958.

[13] Y. Ma, L.H. Yeh, C.Y. Lin, L. Mei, S. Qian, pH-regulated ionic conductance in a nanochannel with overlapped electric double layers, Anal. Chem. 87 (2015) 4508–4514.

[14] J.-P. Hsu, S.-C. Lin, C.-Y. Lin, S. Tseng, Power generation by a pH-regulated conical nanopore through reverse electrodialysis, J. Power Sources 366 (2017) 169–177.
[15] R. Long, Z. Kuang, Z. Liu, W. Liu, Reverse electrodialysis in bilayer nanochannels: salinity gradient-driven power generation, Phys. Chem. Chem. Phys. 20 (2018) 7295–7302.
[16] A. Siria, P. Poncharal, A.L. Biance, R. Fulcrand, X. Blase, S.T. Purcell, L. Bocquet, Giant osmotic energy conversion measured in a single transmembrane boron nitride nanotube, Nature 494 (2013) 455–458.
[17] C. Wang, E. Choi, J. Park, High-voltage nanofluidic energy generator based on ion-concentration-gradients mimicking electric eels, Nano Energy 43 (2018) 291–299.
[18] A. Esfandiar, B. Radha, F.C. Wang, Q. Yang, S. Hu, S. Garaj, R.R. Nair, A.K. Geim, K. Gopinadhan, Size effect in ion transport through angstrom-scale slits, Science 358 (2017) 511–513.
[19] S. Tseng, Y.M. Li, C.Y. Lin, J.P. Hsu, Salinity gradient power: optimization of nanopore size, Electrochim. Acta 219 (2016) 790–797.
[20] Z. Zhang, X.Y. Kong, K. Xiao, Q. Liu, G. Xie, P. Li, J. Ma, Y. Tian, L. Wen, L. Jiang, Engineered asymmetric heterogeneous membrane: a concentration-gradient-driven energy harvesting device, J. Am. Chem. Soc. 137 (2015) 14765.
[21] L. Cao, F. Xiao, Y. Feng, W. Zhu, W. Geng, J. Yang, X. Zhang, N. Li, W. Guo, L. Jiang, Anomalous channel-length dependence in nanofluidic osmotic energy conversion, Adv. Funct. Mater. 27 (2017) 1604302.
[22] Y. Zhang, Y. He, M. Tsutsui, X.S. Miao, M. Taniguchi, Short channel effects on electrokinetic energy conversion in solid-state nanopores, Sci. Rep. 7 (2017) 46661.
[23] S. Tseng, Y.M. Li, C.Y. Lin, J.P. Hsu, Salinity gradient power: influences of temperature and nanopore size, Nanoscale 8 (2016) 2350.
[24] A. Würger, Transport in charged colloids driven by thermoelectricity, Phys. Rev. Lett. 101 (2008) 108302.
[25] D. Vigolo, R. Rusconi, H.A. Stone, R. Piazza, Thermophoresis: microfluidics characterization and separation, Soft Matter 6 (2010) 3489–3493.
[26] T. Ghonge, J. Chakraborty, R. Dey, S. Chakraborty, Electrohydrodynamics within the electrical double layer in the presence of finite temperature gradients, Phys. Rev. E Stat. Nonlinear Soft Matter Phys. 88 (2013) 053020.
[27] J.A. Wood, A.M. Benneker, R.G. Lammertink, Temperature effects on the electrohydrodynamic and electrokinetic behaviour of ion-selective nanochannels, J. Phys. Condens. Matter Inst. Phys. J. 28 (2016) 114002.
[28] A.M. Benneker, H.D. Wendt, R.G.H. Lammertink, J.A. Wood, Influence of temperature gradients on charge transport in asymmetric nanochannels, Phys. Chem. Chem. Phys. 19 (2017) 28232–28238.
[29] D. Vigolo, S. Buzzaccaro, R. Piazza, Thermophoresis and thermoelectricity in surfactant solutions, Langmuir Acs J. Surf. Colloids 26 (2010) 7792.
[30] B.T. Huang, M. Roger, M. Bonetti, T.J. Salez, C. Wiertelgasquet, E. Dubois, R.C. Gomes, G. Demouchy, G. Mériguet, V. Peyre, Thermoelectricity and thermodiffusion in charged colloids, J. Chem. Phys. 143 (2015) 054902.
[31] D. Vigolo, S. Buzzaccaro, R. Piazza, Thermophoresis and thermoelectricity in surfactant solutions, Langmuir ACS J. Surf. Colloids 26 (2010) 7792–7801.
[32] M. Taghipoor, A. Bertsch, P. Renaud, Temperature sensitivity of nanochannel electrical conductance, ACS Nano 9 (2015) 4563.
[33] A.W. Jeffery, M.B. Anne, G.H.L. Rob, Temperature effects on the electrohydrodynamic and electrokinetic behaviour of ion-selective nanochannels, J. Phys. Condens. Matter 28 (2016) 114002.
[34] J. Hwang, T. Sekimoto, W.-L. Hsu, S. Kataoka, A. Endo, H. Daiguji, Thermal dependence of nanofluidic energy conversion by reverse electrodialysis, Nanoscale 9 (2017) 12068–12076.
[35] S. Tseng, Y.-M. Li, C.-Y. Lin, J.-P. Hsu, Salinity gradient power: influences of temperature and nanopore size, Nanoscale 8 (2016) 2350–2357.
[36] A.J. Bard, L.R. Faulkner, Electrochemical methods, fundamental and applications, J. Chem. Educ. 60 (2001) 669–676.
[37] L.A. Bromley, Thermodynamic properties of strong electrolytes in aqueous solutions, Aiche J. 19 (1973) 313–320.
[38] B.B. Owen, R.C. Miller, C.E. Milner, H.L. Cogan, The Dielectric Constant Of Water As A Function Of Temperature And Pressure, J. Phys. Chem. 65 (1961) 2065–2070.
[39] S. Tseng, J.Y. Lin, J.P. Hsu, Theoretical study of temperature influence on the electrophoresis of a pH-regulated polyelectrolyte, Anal. Chim. Acta 847 (2014) 80–89.
[40] J.P. Hsu, Y.H. Tai, L.H. Yeh, S. Tseng, Importance of temperature Effect on the Electrophoretic behavior of charge-regulated particles, Langmuir Acs J. Surf. Colloids 28 (2012) 1013–1019.
[41] P. Pivonka, D. Smith, Investigation of nanoscale electrohydrodynamic transport phenomena in charged porous materials, Int. J. Numer. Methods Eng. 63 (2005) 1975–1990.